PHYSICAL REVIEW A **83**, 042702 (2011)

Electron-collision cross sections for iodine

O. Zatsarinny,[1] K. Bartschat,[1] G. Garcia,[2] F. Blanco,[3] L. R. Hargreaves,[4] D. B. Jones,[4] R. Murrie,[4] J. R. Brunton,[4] M. J. Brunger,[4,5] M. Hoshino,[6] and S. J. Buckman[7]

[1]*Department of Physics and Astronomy, Drake University, Des Moines, Iowa 50311, USA*
[2]*Instituto de Fisica Fundamental, Consejo Superior de Investigaciones Cientificas, Madrid E-28006, Spain*
[3]*Departamento de Fisica Atómica, Molecular y Nuclear, Universidad Complutense de Madrid, Madrid E-28040, Spain*
[4]*ARC Centre for Antimatter-Matter Studies, School of Chemical and Physical Sciences, Flinders University, GPO Box 2100, Adelaide, SA 5001, Australia*
[5]*Institute of Mathematical Sciences, University of Malaya, 50603, Kuala Lumpur, Malaysia*
[6]*Department of Materials and Life Sciences, Sophia University, Chiyoda ku, Tokyo 102-8554, Japan*
[7]*ARC Centre for Antimatter-Matter Studies, Research School of Physics and Engineering, Australian National University, Canberra, ACT 0200, Australia*

(Received 30 January 2011; published 8 April 2011)

We present results from a joint experimental and theoretical study of elastic electron scattering from atomic iodine. The experimental results were obtained by subtracting known cross sections from the measured data obtained with a pyrolyzed mixed beam containing a variety of atomic and molecular species. The calculations were performed using both a fully relativistic Dirac *B*-spline *R*-matrix (close-coupling) method and an optical model potential approach. Given the difficulty of the problem, the agreement between the two sets of theoretical predictions and the experimental data for the angle-differential and the angle-integrated elastic cross sections at 40 eV and 50 eV is satisfactory.

DOI: 10.1103/PhysRevA.83.042702 PACS number(s): 34.80.Dp

I. INTRODUCTION

Interactions between electrons and neutral radicals are known to be one of the key drivers of the chemistry of industrial plasmas [1]. Chemical models to allow for optimized process control of plasma reactors are consequently dependent on the availability of the electron collision cross sections, which give a quantitative understanding of electron interactions with a given target, specifically for the atomic and molecular radicals that are present in the plasma. Despite the importance of such data, quantitative studies of electron collision cross sections with neutral radicals are currently not widely available in the literature [2]. In the absence of such data, optimization and process control techniques for plasma reactors remain mostly empirical, a process which is rapidly showing signs of diminishing returns [1]. In light of this scenario, the plasma fabrication industry and the United States government have committed significant resources [3], in order to develop tools so that a quantitative understanding of plasma reactor behavior and ultimately control might be achieved.

In parallel with the above, transnational agreements such as the Kyoto Protocol have seen the industry look to replace traditional feedstock gases such as CF_4, C_2F_6, C_3F_8, and c-C_4F_8 [4], all of which can be characterized as having a large global warming potential (GWP) [5], with more environmentally friendly alternatives. One such alternative is trifluoroiodomethane (CF_3I), which can be dissociated by electron impact [6,7] and thus can be used as a ready source of CF_3, CF_2, and CF radicals, as well as atomic iodine (I), in the plasma. In addition the C-I bond in CF_3I is relatively weak and hence can also be broken by ultraviolet light [8], leading to it having an atmospheric lifetime in the range of hours to days [7]. This contrasts with CF_4, which is expected to linger in the atmosphere for some 50 000 years [9]. Furthermore, while CF_4 has a GWP about 6500 times that of CO_2 [10], we note that the GWP of CF_3I is only 1–5 times that of CO_2 [5]. Thus CF_3I is an attractive alternative feedstock gas to an industry that still regularly vents those gases into our atmosphere.

The important point in the context of this paper is that in any modeling for CF_3I as a future feedstock gas for use in the semiconductor fabrication industry, electron collision cross sections for atomic iodine will be an essential ingredient. Unfortunately, to the best of our knowledge, no such collision cross sections for elastic and discrete inelastic processes appear to currently exist in the literature. As a consequence, part of the rationale of the present study is to provide an important subset of these cross sections to the plasma modeling community.

This manuscript is structured as follows. We begin in Sec. II by briefly describing the experimental setup, with some emphasis on characterizing the mixed beam on which the measurement is performed. This is followed in Sec. III by a summary of two theoretical methods, the fully relativistic Dirac *B*-spline *R*-matrix (DBSR) method [11] and an optical model potential (OMP) approach [12]. The former is an *ab initio* ansatz based on the close-coupling expansion while the latter effectively corresponds to potential scattering with semiempirical local potentials that are supposed to simulate the effects of polarizing the target's charge cloud and to account for both electron exchange and loss of flux into inelastic channels. Since the OMP method, appropriately modified for molecular effects, will be used to provide cross sections for molecular species such as hydrogen iodide (HI) and I_2 (see below), it is crucial to check the reliability of the method for electron scattering from atomic iodine, for which more sophisticated methods such as the DBSR exist. This comparison, also with the experimental data, is shown in Sec. IV before we conclude with a brief summary.

II. EXPERIMENTAL DETAILS

A. Apparatus

The present apparatus has been described in detail in some of our previous publications (e.g., [13,14]), so that only a brief synopsis is needed here. The apparatus comprised a stainless steel, high-vacuum chamber divided into three differentially pumped stages denoted, respectively, as the source, scattering, and time-of-flight mass spectrometer (TOFMS) chambers. The source stage contained a 0.5 mm nozzle with a 20 mm long silicon carbide (SiC) tube located at the nozzle exit. The SiC tube was resistively heated to temperatures in excess of 1200 °C, as measured by a vanishing filament pyrometer. Atomic iodine was formed by flowing a precursor methyl iodide (CH_3I) gas through the SiC tube, at a driving pressure of ≈430 mbar, pyrolyzing it to yield a "mixed atomic and molecular" beam scattering target. This "mixed" beam contained atomic iodine as well as any other by-products of the pyrolysis. After passage through the SiC tube this mixed beam was cooled under supersonic expansion conditions before the beam centerline was passed to the scattering stage via a 1 mm skimmer, located 3.5 cm downstream of the nozzle. Note that the present supersonic expansion did not employ a buffer gas to aid the expansion, a common practice in most supersonic jet experiments [15]. The reason for this is straightforward. Employing a large excess of buffer gas (as is required) might simply swamp the scattering from our mixed beam, as in an elastic scattering experiment we would not be able to differentiate the contributions from both sources.

The scattering stage of the apparatus contained an electron monochromator [13], which produced the incident electron beam for the collision studies. The electron monochromator comprised a thoriated tungsten filament electron source, a 180° hemispherical energy selector, and electrostatic lenses and deflectors to transport electrons from the filament to the interaction region and form them into a collimated beam. The electron beam energy could be set to any desired value between ∼5–50 eV, although only 40 eV and 50 eV were studied here, with a resolution better than 100 meV [13]. Beam currents from the monochromator, into the interaction region, were typically 5 nA, at the two energies of this study. The electron beam crossed the mixed atomic and molecular beam at right angles, and electrons elastically scattered from the mixed beam were detected by an array of channel electron multipliers (CEMs), each preceded by a retarding field analyzer (RFA) that prevented inelastically scattered electrons from reaching the input plane of the CEM [13]. The energy resolution of the RFA depends on the analyzing energy [16], resulting in a combined monochromator and RFA resolution of approximately 6.5% of the incident beam energy. Output pulses from the CEMs were amplified and registered by standard fast timing and counting circuitry. Data acquisition and analysis were performed under computer control, using custom developed software written under a LabView 8.2 interface. Note that the CEM-RFA detector array consisted of up to eight active detectors, each fixed at a specific scattered electron angle (θ), covering an angular range of 20°–135°. The detectors operate in a parallel, thereby greatly increasing the efficiency of the data collection.

The quantity directly measured here is the elastic differential cross section (DCS) for electrons scattering from the mixed atomic and molecular beam, which we denote as $\sigma_{\rm mix}$. It represents the weighted [for the fractional abundance (I) of a particular component (i) of the mixed beam] sum of the individual DCSs for each of the components in that mixed beam [17]. The measured $\sigma_{\rm mix}$, at a given incident electron energy (E_0) and θ, was placed onto an absolute scale by employing the "pressure drop" skimmed supersonic relative density method (p-SSRDM), as reported by Hargreaves *et al.* [18], whereby the scattering intensity from the target beam is compared with the scattering intensity from a reference beam in order to normalize the cross section. The choice of reference species is theoretically arbitrary, as long as its cross sections are considered known. It is crucial, however, to ensure that the two gas beam fluxes are approximately matched, so that the scattering volume can be considered to be the same for both measurements [18]. In practice, this means that a polyatomic target should be chosen as the reference species in the present study. Hence CF_4, whose DCSs are well known [19,20], was chosen as the reference species for this research. Note also that CF_4 has the added advantage that it does not dissociate at 1250 °C [21], thus allowing for both beams to be prepared with the nozzle at the same temperature.

The final component of our apparatus is the TOFMS stage [13], which houses an orthogonal acceleration, Wiley-McLaren [22], time-of-flight mass spectrometer. Full details on the design and operational performance of the present TOFMS can be found in reference [13]. The TOFMS allowed for mass analysis of the mixed beam, in order to characterize the species formed in the pyrolysis and the relative abundances of those species. The TOFMS utilized a twice frequency-tripled Nd:YAG laser producing photons of wavelength 118 nm (10.48 eV) to single-photon ionize species in the mixed beam. Ionized species were electrically extracted toward a 40 mm multichannel plate detector (MCP) with a timing anode. The MCP anode signal was monitored by a 500 MHz digital oscilloscope (Lecroy 6051A). Ions traveled a total distance of 439.6 mm from the ionization region to the detector, including 350.9 mm of field-free flight. The TOFMS mass resolution was optimized by setting the extraction potentials [13] to achieve a space focus at the MCP [23], that is, ions of the same mass reached the MCP detector at the same time (to a second-order approximation) regardless of their initial spatial position. The TOFMS resolved 1 proton mass differences for molecular masses up to 200 amu. Note that 118 nm photons are not sufficiently energetic to ionize species with a first ionization potential (IP) in excess of 10.48 eV. Any such species present in the mixed beam are accordingly not detected in the present TOFMS, although their abundances might be inferred, as mass is conserved in the pyrolysis process.

B. Mixed-beam characterization

The pyrolysis nozzle was set to a temperature of ∼1250 °C, at which point very little CH_3I was observed (see Fig. 1). Atomic iodine (I), hydrogen iodide (HI), and molecular iodine (I_2) were all also detected in the mixture (again see Fig. 1). The species observed in the present data are in generally good accord with the corresponding TOFMS results reported in Gans *et al.* [15], who employed a SiC nozzle and TOFMS

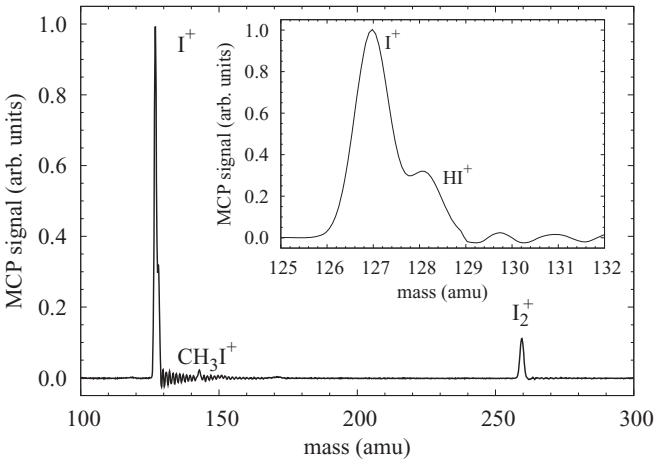

FIG. 1. TOF spectrum for CH_3I pyrolysis, at a nozzle temperature of 1250 °C. The inset shows a zoom around the atomic iodine peak, highlighting the presence of a HI peak. The peaks have each been corrected for their respective photoionization cross section.

configuration similar to ours in order to consider CH_3I pyrolysis over a similar temperature range. A key difference between our result in Fig. 1 and that of Gans *et al.* is that no CH_3 signal is observed by us at the present 1250 °C nozzle temperature. Furthermore, only trace CH_3 quantities (<1%) were observed at the other nozzle temperatures we investigated. Conversely, Gans *et al.* observed significant quantities of CH_3 in their TOFMS data. We attribute this different behavior to the differences in the nozzle geometry and expansion conditions between the two groups. For instance, we employed a longer pyrolysis tube than Gans *et al.* (20 mm compared to 3 mm), worked at a higher driving pressure (430 mbar compared to less than 200 mbar), and did not employ a buffer gas in forming our supersonic expansion. (Gans *et al.* used argon as the buffer gas.) In all cases, these differences dramatically increase the probability of bimolecular reactions in our SiC tube, leading to molecular recombination, compared to the Gans *et al.* arrangement. Accordingly, the lack of CH_3 observed in our TOFMS spectrum is attributed to their collisional recombination within the pyrolysis tube leading to the production of ethane (C_2H_6) molecules:

$$CH_3 + CH_3 \xrightarrow{M} C_2H_6. \quad (1)$$

Here M represents a third body. Note that the IP of C_2H_6 (11.52 eV) is too high for this species to be detected with the present TOFMS, which is why a peak corresponding to its mass is absent in Fig. 1.

The presence of HI in Fig. 1 must also imply some initial formation of CH_2 [15], but in spite of its IP of 10.39 eV we do not observe it in our TOFMS spectra. Similarly, Gans *et al.* did not detect CH_2 in their spectra either, attributing the lack of signal to the very small photoionization cross section of CH_2 at this wavelength. However, given our argument above for C_2H_6 formation, we believe in our case that CH_2 predominately recombines to form ethene (C_2H_4):

$$CH_2 + CH_2 \xrightarrow{M} C_2H_4. \quad (2)$$

Note that C_2H_4 has an IP of 10.51 eV, which is why we do not observe it in our TOFMS. Further note that given we observe some recombined CH_3I, HI, and I_2 (cf. Fig. 1) but do not see any CH_3 or CH_2 in our spectra even though they should be detected if present, our assumption as to the existence of C_2H_4 and C_2H_6 seems sound, since mass must be conserved.

The relative abundance of both C_2H_4 and C_2H_6 can be inferred from mass conservation. The intensity of C_2H_4 is simply given as half that of the measured HI intensity, since two CH_2 molecules are required to form one C_2H_4 molecule and the abundance of CH_2 must equal that of HI [15]. The abundance of C_2H_6 is determined by noting that the amount of CH_3 initially formed must equal half the observed iodine signal, as again two CH_3 molecules are needed for each C_2H_6 molecule to be formed.

In determining the true relative abundances of each species, we must first correct their raw TOFMS signals for their different 118 nm photoionization cross sections. This accounts for the different ionization efficiency of each beam constituent [17]. The relevant photoionization cross sections were taken from Gans *et al.* [15] as 6.7 Mb (atomic I), 48.2 Mb (CH_3I), 74 Mb (I_2), and 44 Mb (HI). Note that the TOFMS data in Fig. 1 have been corrected for this effect. Accordingly, the relative abundance of each species at 1250 °C in the mixed beam is determined as 0.45 ± 0.12 (I), 0.28 ± 0.07 (C_2H_6), 0.14 ± 0.06 (HI), 0.07 ± 0.03 (C_2H_4), 0.05 ± 0.02 (I_2), and 0.010 ± 0.003 (CH_3I). Note that we also considered the possibility for any nonuniform detection efficiency at different ion masses. In our case, however, we believe this efficiency is approximately uniform with respect to mass, as all the ions "hit" the detector with constant energy. This is ensured here as all the ions are extracted by a constant voltage of ~3 kV and they all have a negligible velocity in the TOFMS flight direction when they are ionized by the laser. Finally, further note that 1250 °C was specifically chosen because at around that temperature the relative abundance of atomic iodine in the mixed beam was maximized.

C. Differential cross section measurements

The present mixed-beam differential cross sections at 40 eV and 50 eV are given in Table I. The errors cited on these DCSs are typically of the order of 30% or a little less, including an uncertainty on the reference DCSs (~20%), the uncertainty for our measurement of the change in the pressures (~5%),

TABLE I. DCS measurements for the mixed atomic and molecular beam, in units of 10^{-16} cm^2/sr, at incident energies of 40 and 50 eV. The uncertainties on the DCS data are quoted at the one standard deviation level.

	50 eV		40 eV	
Scattering Angle (deg)	σ	$\Delta\sigma$	σ	$\Delta\sigma$
20	9.60	2.80	10.7	3.20
40	0.45	0.12	0.53	0.16
60	0.38	0.11	0.50	0.15
75	0.46	0.14	0.46	0.14
90	0.16	0.05	0.15	0.05
105	0.84	0.31	0.60	0.21
120	1.78	0.54	1.06	0.33
135	1.59	0.47	0.82	0.25

the uncertainty in the pumping speed calibration (∼5%), the uncertainty in matching the spatial distribution of both the reference and mixed-beam gases (∼10%), as well as the statistical variation in the elastically scattered signal for each angle and energy for both respective gases. All the errors in Table I are reported at the one standard deviation level. When we originally began these measurements, it was our intention to study the DCSs for a larger range of incident electron energies than the two we report. Unfortunately, the mixed beam containing about 50% of I and I_2 seriously affected the performance of the source chamber diffusion and backing pumps. This is in spite of our use of nonreactive Fomblin oils in both those pumps. The replacement of such quantities of oil in these pumps was an expensive undertaking and consequently curtailed the scope of our experimental investigations. In addition, the source chamber surfaces quickly coated with a yellow film that required extensive cleaning to remove. This also mitigated against further measurements.

To the best of our knowledge there are no other measurements or calculations against which we can compare our values for $\sigma_{\rm mix}$. This, however, is not surprising, as the values of $\sigma_{\rm mix}$ depend on the temperature at which they are measured. Note that the relative abundances (I_i) of the various species (i) that constitute the mixed beam are strongly temperature dependent [17]. Nonetheless, these data may have some practical relevance to scientists attempting to model the behavior of a CH_3I low-temperature plasma. To first order, the species present in such a plasma are mimicked by our mixed beam, so that the cross sections we measure might have application in such a modeling study. Both our 40 eV and 50 eV mixed-beam DCSs are strongly peaked in magnitude (see Table I) when going toward forward scattering angles. Such behavior is consistent [24] with the atomic (I) and molecular (CH_3I, HI, I_2, C_2H_4, C_2H_6) species present having dipole polarizabilities of significant magnitude and/or a strong permanent dipole moment.

As we noted earlier, the mixed-beam DCS represents the weighted sum of each of the individual species DCSs (σ_i) that comprise that beam. Mathematically, we write this as

$$\sigma_{\rm mix} = \sum_i I_i \sigma_i . \tag{3}$$

For the particular case of this study, Eq. (3) can be explicitly expanded by

$$\sigma_{\rm mix} = 0.45\,\sigma_{\rm I} + 0.28\,\sigma_{C_2H_6} + 0.14\,\sigma_{\rm HI} + 0.07\,\sigma_{C_2H_4} + 0.05\,\sigma_{I_2} + 0.01\,\sigma_{CH_3I},$$

which we can further rearrange, now also including the uncertainties on the abundances, to give

$$\sigma_{\rm I} = \frac{1}{(0.45 \pm 0.12)} [\sigma_{\rm mix} - (0.28 \pm 0.07)\,\sigma_{C_2H_6} - (0.14 \pm 0.06)\,\sigma_{\rm HI} - (0.07 \pm 0.03)\,\sigma_{C_2H_4} - (0.05 \pm 0.02)\,\sigma_{I_2} - (0.01 \pm 0.003)\,\sigma_{CH_3I}]. \tag{4}$$

Hence, it is immediately apparent from Eq. (4) that—provided the DCSs for the mixed beam, ethane, hydrogen iodide, ethene, molecular iodine, and methyl iodide are known—the DCSs for atomic iodine can be determined. The DCS measurements for C_2H_6 and C_2H_4 were taken from the data compilation of Hoshino *et al.* [25], while those for CH_3I came from our own measurements [26]. Unfortunately, we do not know of any experimental DCSs for electron scattering from either I_2 or HI. As a consequence of this we computed them from independent atom model calculations, employing an optical model potential [12] (see below). A screening-corrected additivity rule (SCAR) [12] was further applied to the independent atom model (IAM) results, in order to incorporate the effects of the molecular geometry into the calculation. There is growing evidence ([24,26] and references therein) that, at least for energies greater than about 40 eV (or perhaps even lower), the IAM-SCAR approach can provide accurate and reliable DCS and integral cross section (ICS) data. As a consequence, we believe its use in conjunction with Eq. (4) for $\sigma_{\rm HI}$ and σ_{I_2} should be reasonably valid. Since HI and I_2 only constitute ∼19% of the mixed beam, the IAM-SCAR theoretical cross sections would have to be seriously inaccurate to have a major deleterious effect on the values of $\sigma_{\rm I}$ that we are trying to determine. Indeed, even if our theoretical values were incorrect by as much as a factor of two, this would only result in a ∼30% change to our extracted cross sections for atomic iodine. This is well within the uncertainties we quote. In any event, the existing evidence clearly suggests that our theoretical results for HI and I_2 are unlikely to be seriously inaccurate at 40 and 50 eV.

One of the limitations with our experimental approach is that every time we subtract one of the constituent species cross sections from that of the mixed-beam cross sections, the residual values get progressively smaller while their associated uncertainties compound and become progressively larger. This is an inherent problem with "difference" experiments such as the present. In addition, while we have mounted an argument above as to why in general our IAM-SCAR results should be reliable we have no specific independent results to confirm that assertion for HI and I_2. Therefore the uncertainties we quote on our derived atomic iodine differential cross sections are at the two standard deviation level. We believe that given the inherent difficulties associated with what is a very challenging

TABLE II. DCS and ICS measurements for elastic electron scattering from atomic iodine, in units of 10^{-16} cm^2/sr and 10^{-16} cm^2, respectively, at incident energies of 40 and 50 eV. The uncertainties for the DCS data are quoted at the two standard deviation level, while an 80% one standard deviation uncertainty has been attributed to the ICS data.

	50 eV		40 eV	
Scattering Angle (deg)	σ	$\Delta\sigma$	σ	$\Delta\sigma$
20	14.0	13.7	16.0	15.7
40	0.32	0.57	0.52	0.51
60	0.47	0.46	0.59	0.58
75	0.82	0.61	0.72	0.66
90	0.22	0.13	0.19	0.13
105	1.60	1.57	1.00	0.98
120	3.60	3.10	1.90	1.80
135	3.30	2.80	1.60	1.40
ICS	27.0	22.0	25.0	20.0

experiment, quoting uncertainties at the two standard deviation level is both prudent and realistic.

In Table II we therefore list our present 40 and 50 eV elastic differential cross sections, and their associated errors, for electrons scattering from atomic iodine. To the best of our knowledge, these represent the only measured data reported for this scattering system to date. Also listed at the bottom of Table II are estimates of the current elastic ICS at both energies. These ICS data were determined from the DCS results by using a molecular phase shift analysis (MPSA) procedure [27], in order to extrapolate the measurements to 0° and 180° and perform the usual integration. The errors on the ICS that we cite are at the one standard deviation level, typically of the order of 80%. Such a large error reflects both the magnitude of the one standard deviation uncertainties on the differential cross sections and a rather large uncertainty associated with our extrapolation procedure in this case. As can be seen from Fig. 2, the DCSs for atomic iodine are strongly peaked toward forward scattering angles. Even allowing for the $\sin\theta$ weighting factor in the calculation of the ICS, the contribution to the integrand at $\theta < 20^\circ$, where we have no data, is significant. Thus the value of the ICS we determine is particularly sensitive to the MPSA extrapolation for $\theta < 20^\circ$, a fact which is reflected in the size of the ICS errors we quote.

III. NUMERICAL APPROACHES

As mentioned above, two numerical approaches were employed to predict the cross sections of interest. These are the fully relativistic Dirac B-spline R-matrix (DBSR) method [11] and an optical model potential (OMP) approach [12]. The main features of the calculations will be described below, including the extension of the OMP approach to treat scattering from molecules.

A. DBSR calculations

The DBSR calculations are based on the method described by Zatsarinny and Bartschat [11]. Since we are interested in elastic scattering, a very important effect to account for is the polarization of the atomic charge cloud due to the projectile. On the other hand, coupling to individual excited states is less important, as long as their contribution to the polarizability of the ground state is accounted for in some way.

Consequently, we set up the close-coupling expansion including only two physical states, namely those with the $5s^2 5p^5$ ground-state configuration and total electronic angular momenta $J = 3/2$ and $J = 1/2$, respectively. In order to account for the polarizability of these states, we then generated three pseudostates with configurations $5s^2 5p^4 \bar{6}s + 5s^2 5p^4 \bar{5}d$ ($J = 1/2,3/2,5/2$) and another two with configurations $5s^2 5p^4 \bar{6}s + 5s^2 5p^4 \bar{5}d$ ($J = 1/2,3/2$). Coupling of the former to the $5s^2 5p^5 (J = 3/2)$ state and of the latter to the $5s^2 5p^5 (J = 1/2)$ state yielded dipole polarizabilities of $\alpha_d = 35.2\, a_0^3$ and $\alpha_d = 36.6\, a_0^3$, respectively, in excellent agreement with the values of $\alpha_d = 34.6\, a_0^3$ and $\alpha_d = 35.1\, a_0^3$ obtained in high-precision structure-only calculations [28]. (Here $a_0 = 0.529 \times 10^{-10}$ m is the Bohr radius.) Achieving such a good target description is possible because of our ability to use separately optimized, and hence nonorthogonal, orbitals for all these states.

We then used the recently developed DBSR program [11] to solve the $(N+1)$-electron collision problem. The essential idea is to expand the basis of continuum orbitals used to describe the projectile electron inside the R-matrix box, i.e., the region where the problem is most complicated due to the highly correlated motion of $N+1$ electrons, also in terms of a B-spline basis. A semiexponential grid for the B-spline knot sequence was set up to cover the inner region up to the R-matrix radius a. We used the same grid for the structure and the collision calculations. For $a = 50\, a_0$, we employed 111 splines. A tight knot distribution near the origin was necessary to incorporate a finite-size nuclear model with a Fermi potential.

We calculated partial-wave contributions up to $J = 51/2$ numerically. With such a high value of J, no extrapolation scheme to account for even higher partial waves was necessary for all DBSR results presented in this paper. The cross sections of interest were calculated in the same way as in the standard R-matrix approach. We employed an updated version [29] of the flexible asymptotic R-matrix (FARM) package by Burke and Noble [30] to solve the problem in the asymptotic region and to obtain the transition matrix elements of interest. After transforming the latter from the present jj-coupling to the jlK-coupling scheme and also accounting for the appropriate phase convention of the reduced matrix elements, we employed the program MJK of Grum-Grzhimailo [31] to calculate the angle-differential cross sections (DCS).

B. OMP calculations

The OMP model is essentially a potential scattering approach. Using atomic units with k^2 denoting the energy in rydberg, we solve the partial-wave equation

$$\left(\frac{d^2}{dr^2} - \frac{\ell(\ell+1)}{r^2} - 2V_{\rm mp}(k,r)\right) u_\ell(k,r) = k^2 u_\ell(k,r), \quad (5)$$

where the local model potential is taken as

$$V_{\rm mp}(k,r) = V_{\rm st}(r) + V_{\rm ex}(k,r) + V_{\rm pol}(r) + i\, V_{\rm abs}(k,r). \quad (6)$$

Here $V_{\rm st}(r)$ is the standard Hartree potential of the target. It is then supplemented by the exchange potential $V_{\rm ex}(k,r)$ used by Riley and Truhlar [32], the polarization potential $V_{\rm pol}(r)$ employed by Zhang *et al.* [33], and finally the imaginary absorption potential $i\, V_{\rm abs}(k,r)$ of Staszewska *et al.* [34].

Due to the imaginary absorption potential, the OMP method yields a complex phase shift $\delta_\ell = \lambda_\ell + i\,\mu_\ell$. This allows for the calculation of cross sections for elastic scattering, inelastic scattering (all excited and ionized states lumped together), and the grand total as the sum of the two processes.

As mentioned in the previous section, the OMP model was also used in the present work to estimate the respective cross sections for electron collisions with molecular iodine (I_2) as well as the HI component of the mixed beam. This was done via a "screening corrected additivity rule" (SCAR) approach. The general idea is to add the cross sections from scattering by the individual atoms in the molecule, but then incorporate translation and screening factors to account for the molecular

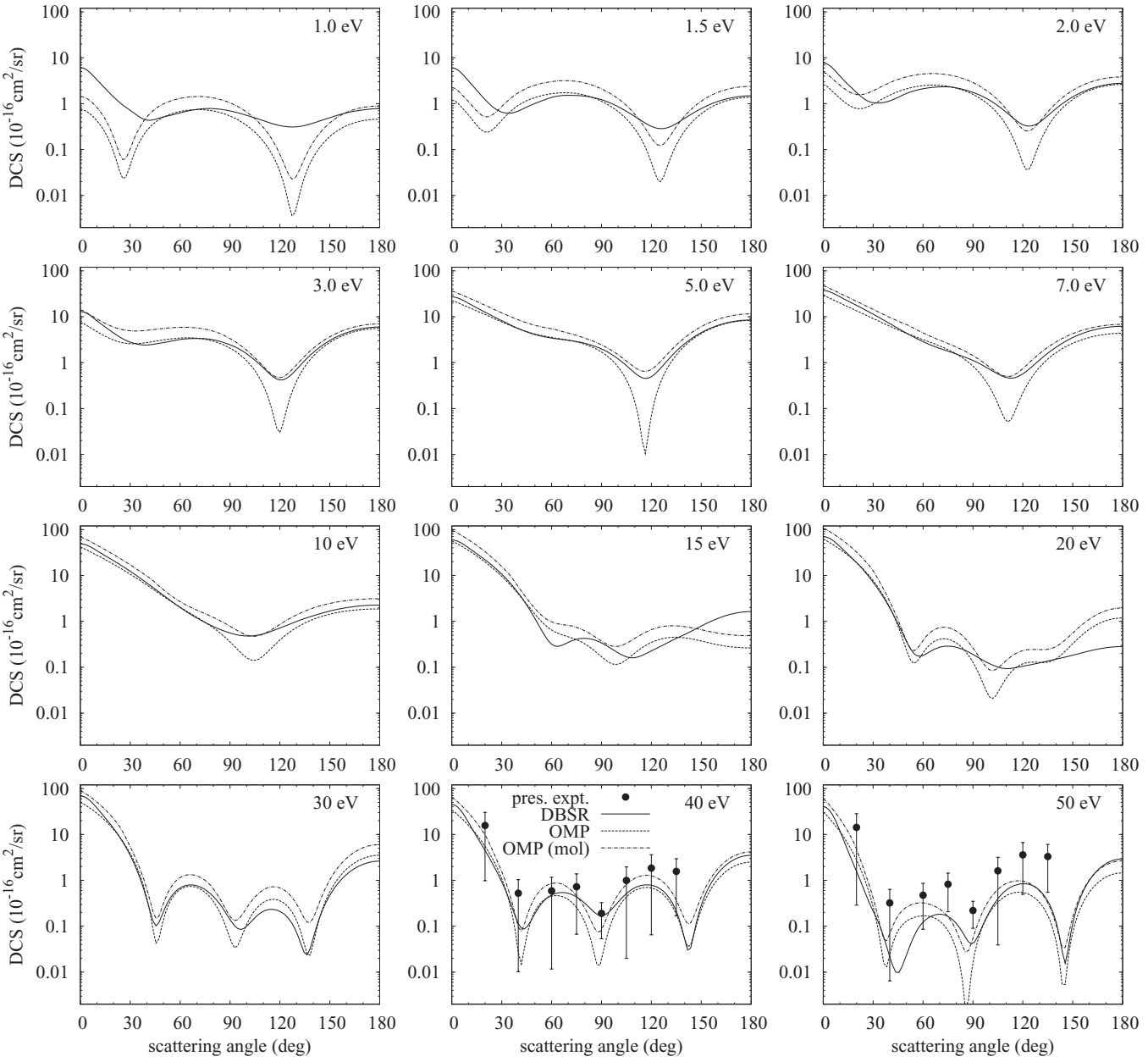

FIG. 2. Elastic DCS for atomic iodine in units of 10^{-16} cm^2/sr, at incident energies between 1 eV and 50 eV. The error bars in the experimental data at 40 eV and 50 eV represent a two standard deviation uncertainty. Also shown are calculated results employing the DBSR (solid curve) and OMP (dashed curve) approaches, as well as the OMP predictions for molecular iodine.

geometry. Details of this OMP-SCAR model were given by Blanco and Garcia [12].

IV. RESULTS

Figure 2 exhibits the *e*-I elastic cross sections for twelve energies between 1 eV and 50 eV, as predicted by the DBSR and OMP models. For 40 eV and 50 eV, the experimental results reported in Table II are shown as well. Recall that the uncertainties in the experimental data represent the quadrature sum of counting statistics, uncertainties in the abundances of each species, and the uncertainties in the DCS values for the beam constituents, including the results for I_2 that are also shown in the figure. In the case of HI and I_2, an uncertainty of 20% was used for those DCSs at 40 eV and 50 eV. Since the present data require subtraction of a large number of quantities, several of which themselves have substantive uncertainties, the experimental data presented in Fig. 2 show error bars at the two standard deviation level.

The present measurements are in excellent shape agreement with theory at both 40 eV and 50 eV, particularly with respect to the locations of the minima in the DCS. The calculated magnitude of the DCS is also in reasonable agreement with the experimental data at 40 eV, while at 50 eV the measured data are uniformly larger than predicted by either calculation.

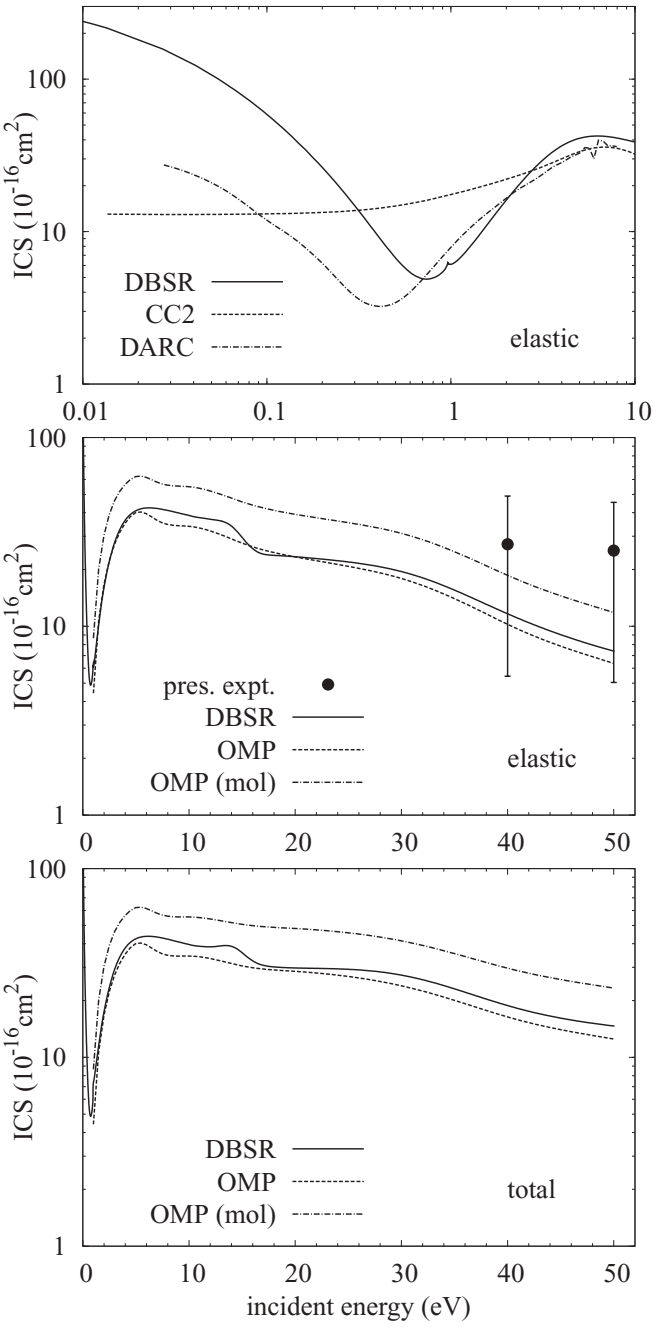

FIG. 3. Absolute ICS for iodine atoms, in units of 10^{-16} cm^2. The top and center panels show the angle-integrated elastic results while the bottom panel depicts the total cross section. The error bars in the two experimental data points represent a one standard deviation uncertainty, estimated to be 80%. Also shown are predictions from various theories described in the text. Note that the published results of Wu and Yuan [35] were multiplied by 100, since there was a plotting error in their paper [36].

Except for the very small energies, and in the depth of some of the minima as well as their position, the agreement between the DBSR and OMP results is satisfactory. This is important, since it provides, albeit indirectly, some confidence in the predictions of the OMP model for the cross sections for scattering from the molecular species I_2. As seen from the panels, the OMP results for I_2 are similar in shape but generally larger than those for atomic iodine. However, the ratio between the molecular and the atomic DCS is not simply a factor of two, since the molecular geometry has been accounted for.

Figure 3 shows the corresponding angle-integrated cross sections, both for the elastic channel alone and for the total, i.e., the sum of elastic and all inelastic contributions. The DBSR model predicts the Ramsauer minimum around 0.7 eV. In contrast, Wu and Yuan [35] obtained the minimum around 0.4 eV in their 11-state fully relativistic Dirac-based calculation. Note that the results presented from the latter paper should be multiplied by 100 because of a unit error [36]. The OMP calculations also support the existence of the minimum, although the lowest collision energy (1.0 eV) treated in the present work is not low enough to map out the minimum. On the other hand, a standard two-state close-coupling model (CC2), which only couples the $5s^25p^5$ ($J = 3/2,1/2$) states and hence does not account for the full dipole polarizability, shows no Ramsauer minimum at all.

V. SUMMARY

We have presented results from a joint experimental and theoretical study of elastic electron scattering from atomic iodine. The experimental data were extracted from a measurement on a mixed beam that contained a variety of atomic and molecular species after pyrolysis of CH_3I. We found satisfactory agreement between the measurements and predictions from two independent calculations. This gives us confidence that our elastic DBSR results would be suitable for use in modeling plasma kinetic behavior for any plasma in which atomic iodine is a constituent. Our DBSR calculation could also be extended to provide cross sections for electron impact excitation of individual discrete levels. Those discrete inelastic cross sections, which are not available from the OMP approach, would also be of interest to the plasma modeling community.

The present comparison between theory and experiment is also encouraging since it suggests that the general strategy of this mixed-beam setup will work for other targets as well. Furthermore, the OMP-SCAR model seems sufficiently accurate to be used for the calculations of otherwise hard-to-find cross sections, particularly for e-I_2 collisions.

ACKNOWLEDGMENTS

This work was supported in part by the United States National Science Foundation under Grants No. PHY-0757755 (K.B.) and No. PHY-0903818 (O.Z. and K.B.) and supercomputer resources through the NSF TeraGrid Allocation Award No. TG-PHY090031. The Australian Research Council, through its Centres of Excellence program, is also thanked for some financial support. Additional support from the Ministerio de Ciencia e Innovacion (Project No. FISI2009-102345) and the European Science Foundation (COST Action CM0601) is acknowledged. One of us (M.H.) also thanks the Researcher Exchange Program between JSPS and AAS for his grant to visit Flinders University and the ANU.

[1] D. B. Graves, M. J. Kushner, J. W. Gallagher, A. Garscadden, G. S. Oerlein, and A. V. Phelps, *Database Needs for Modelling and Simulation of Plasma Processing* (National Research Council, National Academy Press, Washington, DC, 1996).
[2] N. J. Mason, J. Phys. D **42**, 11 (2009).
[3] M. J. Kushner, Bull. Am. Phys. Soc. **55**, 107 (2010).
[4] S. Raoux *et al.*, J. Vac. Sci. Technol. B **17**, 477 (1999).
[5] L. G. Christophorou and J. K. Olthoff, J. Phys. Chem. Ref. Data **29**, 553 (2000).
[6] Y. Li, K. O. Patten, D. Youn, and D. J. Wuebbles, Atmos. Chem. Phys. **6**, 4559 (2006).
[7] H. Cho, M. Y. Song, J. S. Yoon, M. Hoshino, and H. Tanaka, J. Phys. B **43**, 135205 (2010).
[8] M. H. F. Bettega, A. P. P. Natalense, M. A. P. Lima, and L. G. Ferreira, J. Phys. B **36**, 1263 (2003).
[9] I. Rozum, P. Limao-Vieira, S. Eden, J. Tennyson, and N. J. Mason, J. Phys. Chem. Ref. Data **35**, 267 (2006).
[10] T. Tanaka, M. Hoshino, H. Kato, J. R. Harries, Y. Tamenori, K. Ueda, and H. Tanaka, J. Electron Spectrosc. Relat. Phenom. **164**, 24 (2008).
[11] O. Zatsarinny and K. Bartschat, Phys. Rev. A **77**, 062701 (2008).
[12] F. Blanco and G. Garcia, Phys. Lett. A **317**, 458 (2003).
[13] T. M. Maddern, L. R. Hargreaves, M. Bolorizadeh, M. J. Brunger, and S. J. Buckman, Meas. Sci. Technol. **19**, 085801 (2008).
[14] J. R. Francis-Staite, T. M. Maddern, M. J. Brunger, S. J. Buckman, C. Winstead, V. McKoy, M. A. Bolorizadeh, and H. Cho, Phys. Rev. A **79**, 052705 (2009).
[15] B. Gans *et al.*, J. Phys. Chem. A **114**, 3237 (2010).
[16] J. A. Simpson, Rev. Sci. Instrum. **32**, 1283 (1961).
[17] L. R. Hargreaves, J. R. Brunton, M. J. Brunger, and S. J. Buckman, Plasma Sources Sci. Technol. **19**, 065021 (2010).
[18] L. R. Hargreaves, J. R. Francis-Staite, T. M. Maddern, M. J. Brunger, and S. J. Buckman, Meas. Sci. Technol. **18**, 2783 (2007).
[19] L. Boesten, H. Tanaka, A. Kolayashi, M. A. Dillon, and M. Kimura, J. Phys. B **25**, 1607 (1992).
[20] J.-S. Yoon, M.-Y. Song, H. Kato, M. Hoshino, H. Tanaka, M. J. Brunger, S. J. Buckman, and H. Cho, J. Phys. Chem. Ref. Data **39**, 033106 (2010).
[21] T. M. Maddern, L. R. Hargreaves, J. R. Francis-Staite, M. J. Brunger, S. J. Buckman, C. Winstead, and V. McKoy, Phys. Rev. Lett. **100**, 063202 (2008).
[22] W. C. Wiley and I. H. McLaren, Rev. Sci. Instrum. **26**, 1150 (1955).
[23] U. Boesl, R. Weinkauf, and E. W. Schlag, Int. J. Mass Spectrom. **112**, 121 (1992).
[24] H. Kato *et al.*, J. Chem. Phys. **132**, 074309 (2010).
[25] M. Hoshino *et al.*, Research Report No. 101, NIFS-Data Series (National Institute for Fusion Science, Tokyo, Japan, 2008).
[26] L. R. Hargreaves, J. R. Brunton, A. Prajapati, M. Hoshino, F. Blanco, G. Garcia, S. J. Buckman, and M. J. Brunger, J. Phys. B **44**, 045207 (2011).
[27] L. Campbell, M. J. Brunger, A. M. Nolan, L. J. Kelly, A. B. Wedding, J. Harrison, P. J. O. Teubner, D. C. Cartwright, and B. McLaughlin, J. Phys. B **34**, 1185 (2001).
[28] T. Fleig and A. J. Sadlej, Phys. Rev. A **65**, 032506 (2002).
[29] C. J. Noble (private communication).
[30] V. M. Burke and C. J. Noble, Comput. Phys. Commun. **85**, 471 (1995).
[31] A. N. Grum-Grzhimailo, Comput. Phys. Commun. **152**, 101 (2003).
[32] M. E. Riley and D. G. Truhlar, J. Chem. Phys. **63**, 2182 (1975).
[33] X. Zhang, J. Sun, and Y. Liu, J. Phys. B **25**, 1893 (1992).
[34] G. Staszewska, D. W. Schwenke, D. Thirumalai, and D. G. Truhlar, Phys. Rev. A **28**, 2740 (1983).
[35] J. Wu and J. Yuan, Phys. Rev. A **76**, 024702 (2007).
[36] J. Yuan (private communication).